Modeling Microwave Structures in Time Domain Using Laguerre Polynomials

Jaroslav LÁČÍK, Zbyněk RAIDA

Dept. of Radio Electronics, Brno University of Technology, Purkyňova 118, 612 00 Brno, Czech Republic

lacik@feec.vutbr.cz, raida@feec.vutbr.cz

Abstract. *The paper is focused on time domain modeling of microwave structures by the method of moments. Two alternative schemes with weighted Laguerre polynomials are presented. Thanks to their properties, these schemes are free of late time oscillations.*

Further, the paper is aimed to effective and accurate evaluation of Green's functions integrals within these schemes. For this evaluation, a first- and second-order polynomial approximation is developed.

The last part of the paper deals with modeling microstrip structures in the time domain. Conditions of impedance matching are derived, and the proposed approach is verified by modeling a microstrip filter.

Keywords

Time domain analysis, method of moments, Laguerre polynomials, microstrip structures.

1. Introduction

Electric field integral equations (EFIE) are widely used for the numerical analysis of electromagnetic radiation and scattering. Essentially, when broad-band information is desired, the time domain (TD) solution of the electromagnetic (EM) problem is more efficient. Several formulations have been presented for TD-EFIE [1], [2], [3]. The explicit scheme and the implicit one have attracted the most attention. These approaches are called the marching-on in time (MOT) methods.

The explicit scheme suffers from the late-time instability, which usually takes the form of exponentially increasing oscillations alternating in sign at each time step. In [1], the implicit scheme is proposed in order to suppress the instability. The implicit scheme is advantageous, but the late time oscillations are not eliminated totally [3]. Moreover, the implicit scheme is less accurate than the explicit one.

In [4], the unconditionally stable solution exploiting Laguerre polynomials was proposed. The causal weighted Laguerre polynomials [4] were used as temporal basis and testing functions. There are five characteristic properties of the weighted Laguerre polynomials: they are (1) causal, (2) recursively computed, (3) orthogonal, (4) convergent, and (5) separating space and time variables. This scheme does not suffer from the late time instability, but is less efficient.

In this paper, two alternative schemes with weighted Laguerre polynomials are presented. The first one was introduced in [7], and the second one has been its alternative formulation. Both the schemes use neither the auxiliary vector [4] as an unknown quantity representing the electric current density, nor the derivative of the electric field intensity of the incident wave.

The paper is organized as follows. Section 2 presents the basic EFIE formulation in the time domain. Section 3 describes the alternative schemes based on weighted Laguerre polynomials. In section 4, an efficient and accurate evaluation of Green's function integrals is discussed, when sums of weighted Laguerre polynomials are approximated by first- and second-order polynomials. Section 5 is focused on modeling microstrip structures in the time domain, and Section 6 concludes the paper.

2. TD-EFIE Formulation

Let S denote the surface of a perfectly electrically conducting (PEC) body illuminated by a transient electromagnetic wave. The incident wave induces a surface current $\mathbf{J}(\mathbf{r}, t)$ on S. The scattered electric field $\mathbf{E}^S(\mathbf{r}, t)$ computed from the surface current is given by

$$\mathbf{E}^S = -\frac{\partial \mathbf{A}}{\partial t} - \nabla \phi \;, \tag{1}$$

where $\mathbf{A}$ is the magnetic vector potential and ϕ denotes the electric scalar potential defined by

$$\mathbf{A}(\mathbf{r}, t) = \frac{\mu}{4\pi} \int_S \frac{\mathbf{J}(\mathbf{r}', \tau)}{R} dS' \;, \tag{2}$$

$$\phi(\mathbf{r}, t) = \frac{1}{4\pi\varepsilon} \int_S \frac{q(\mathbf{r}', \tau)}{R} dS' \;. \tag{3}$$

The permeability and the permitivity of the surrounding medium are $\mu = \mu_r \mu_0$ and $\varepsilon = \varepsilon_r \varepsilon_0$, respectively, the

symbol $R = |\mathbf{r} - \mathbf{r}'|$ denotes the distance between an arbitrarily located observation point $\mathbf{r}$ and a source point $\mathbf{r}'$ on S, and $\tau = t - R/c$ is the retarded time. The velocity of the propagation in the surrounding medium is $c = (\mu\varepsilon)^{-1/2}$. The charge density q on the surface S is related to the current density $\mathbf{J}$ on the same surface by the continuity theorem:

$$q(\mathbf{r},t) = -\int_0^t \nabla \cdot \mathbf{J}(\mathbf{r},t')\, dt' \ . \tag{4}$$

Substituting (4) to (3), we get

$$\phi(\mathbf{r},t) = -\frac{1}{4\pi\varepsilon}\iint_{S\ 0}^{\ \ t}\frac{\nabla' \cdot \mathbf{J}'(\mathbf{r}',t')}{R}\, dt'\, dS' \ . \tag{5}$$

Since the total tangential electric field is zero on the conducting surface for all time instants, we get

$$\left[\mathbf{E}^i + \mathbf{E}^S(\mathbf{J})\right]_{\tan} = 0, \quad \mathbf{r} \in S \ , \tag{6}$$

$$\left[\partial \mathbf{A}/\partial t + \nabla\phi\right]_{\tan} = \left[\mathbf{E}^i\right]_{\tan} \ , \tag{7}$$

where $\mathbf{E}^i$ is the incident electric field on the scatterer, and the subscript "tan" denotes the tangential component. The equation (7) completed by (2) and (5) constitutes TD-EFIE. Solving it, the unknown current $\mathbf{J}(\mathbf{r}, t)$ may be determined.

To be noticed, quantities with an apostrophe are related to an observation point, and quantities without an apostrophe are related to a source point in this paper.

3.   TD-EFIE Using Weighted Laguerre Polynomials: Alternative Schemes

The equation (7) is solved by the method of moments (MoM) [1]. The PEC surfaces of the analyzed structure are approximated by planar triangular patches and Rao-Wilton-Glisson (RWG) functions [5] are used to expand the spatial variation of the electric current density. The unknown current density $\mathbf{J}(\mathbf{r}, t)$ is approximated as

$$\mathbf{J}(\mathbf{r},t) = \sum_{n=1}^{N} I_n(t)\, \mathbf{f}_n(\mathbf{r}) \ , \tag{8}$$

$$\mathbf{f}_n = \begin{cases} \dfrac{l_n}{2A_n^{\pm}}\boldsymbol{\rho}_n^{\pm}, & \mathbf{r} \in T_n^{\pm} \\[2mm] \mathbf{0}, & otherwise \end{cases} \tag{9}$$

where $I_n(t)$ is the unknown temporal current coefficient on the n-th edge of the triangular mesh, l_n is the length of the n-th edge, $A_n^{\pm}$ denotes the area of the triangle $T_n^{\pm}$, $\boldsymbol{\rho}_n^{\pm}$ is the vector from respectively to the free vertex of $T_n^{\pm}$ to respectively from the observation point $\mathbf{r}$ and N is the number of non-boundary edges. The functions $\mathbf{f}_n$ (9) are called RWG functions. A boundary edge is defined as an edge, which is associated with a single triangular patch (Fig. 1).

In the following steps, we substitute the current density approximation (8) to the vector potential (2), and to the scalar potential (5). Then, the potentials are substituted into (7); Galerkin's method and the centroidal testing scheme are applied (this spacious testing procedure is the same as in [5]). This yield:

$$\sum_{n,p,o}\left[\mathbf{K}_{mn}^{po}(\mathbf{r}_m^c) \cdot \int_{T_n^o} \frac{\delta I_n\left(t - R_{mn}^p/c\right)}{\delta t}\frac{\boldsymbol{\rho}_n^o(\mathbf{r}_n^c)}{R_{mn}^p}\, dS' \right.$$
$$\left. \pm L_{mn}^{po}\int_{T_n^o}\frac{\int I_n\left(t-R_{mn}^p/c\right)dt}{R_{mn}^p}\, dS' \right] = V_m(t) \tag{10}$$

where

$$\sum_{n,p,o} \equiv \sum_{n=1}^{N}\sum_{p=1}^{2}\sum_{o=1}^{2} \ , \tag{11}$$

$$\mathbf{K}_{mn}^{po}(\mathbf{r}_m^c) = \frac{\mu l_m}{16\pi}\,\boldsymbol{\rho}_m^p(\mathbf{r}_m^c)\frac{l_n}{A_n^o} \ , \tag{12}$$

$$L_{mn}^{po} = \frac{l_m}{4\pi\varepsilon}\frac{l_n}{A_n^o} \ , \tag{13}$$

$$\begin{aligned} V_{m=h}(t) &= l_h U(t) \quad for\ m = h \\ V_m(t) &= 0 \qquad\qquad otherwise \end{aligned} \ , \tag{14}$$

$$R_{mn}^p = \left| \mathbf{r}_m^c - \mathbf{r}'_n \right| \ . \tag{15}$$

In case of the superscript po, $p = o$ symbolizes "+", and $p \neq o$ symbolizes "–" (the meaning of the sing in front of the integral in eqn. 10). In case of the superscript p or the superscript o, the values $p = 1$, $o = 1$ symbolize the superscript "+", and the values $p = 2$, $o = 2$ symbolize the superscript "–". The superscript c denotes a value, which is related to the centroid of the triangular patch. The equation (14) was derived with the assumption, that the delta-function generator (the edge feeding model) is applied as a voltage source $U(t)$ at the h-th edge [8].
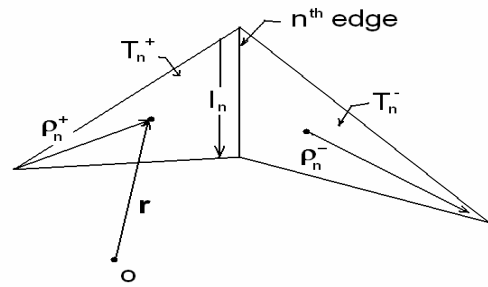
Fig. 1. Definition of the RWG function.

The unknown temporal coefficients $I_n(t)$ can be expanded using weighted Laguerre polynomials

$$I_n(t) = \sum_{u=0}^{\infty} I_{n,u}\, \varphi_u(st) \ , \tag{16}$$

where

$$\varphi_u(st) = \exp(-st/2)\, L_u(st) \ . \tag{17}$$

Further, $s > 0$ is a time scale factor, and L_u is Laguerre polynomial of order u defined recursively by

$$L_0(t) = 1 , \quad L_1(t) = 1 - t , \tag{18}$$

$$u L_u(t) = (2u - 1 - t) L_{u-1}(t) - (u - 1) L_{u-2}(t) \tag{19}$$
$$\text{for } u \geq 2, t \geq 0 .$$

For solving the equation (10), the first derivative and the integral (with respect to t) of the unknown temporal coefficients $I_n(t)$ given by (17) have to be evaluated. The first derivative can be expressed by following two relations [6]

$$\frac{\partial I_n(t)}{\partial t} = -\frac{s}{2} \sum_{u=0}^{\infty} I_{n,u} \left[\varphi_u(st) + \sum_{k=0}^{u-1} \varphi_k(st) \right] , \tag{20a}$$

$$\frac{\partial I_n(t)}{\partial t} = -\frac{s}{2} \sum_{u=0}^{\infty} \left[I_{n,u} + 2\sum_{k=0}^{u-1} I_{n,k} \right] \varphi_u(st) , \tag{20b}$$

and the integral by

$$\int I_n(t)\, dt = \tag{21}$$
$$= -\frac{2}{s} \sum_{u=0}^{\infty} I_{n,u} \left[\varphi_u(st) - 2d \sum_{k=0}^{u-1} (-1)^k \varphi_k(st) \right] ,$$

where $d = 1$ for even u, and $d = -1$ for odd u.
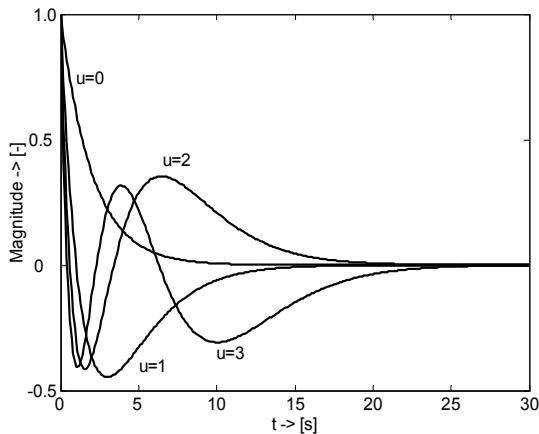
Fig. 2. Weighted Laguerre polynomials of different orders.

Substituting (20) and (21) into (10), multiplying both sides of (10) by $\varphi_v(st)$, integrating over $t = [0, \infty>$, which represents the temporal testing procedure in a fact, and considering the orthogonal property of the weighted Laguerre function, we obtain alternative two formulations

$$\sum_{n,p,o} \left[\frac{-s}{2} \mathbf{K}_{mn}^{po}(\mathbf{r}_m^c) \cdot \int_{T_n^o} \frac{a_{mn}^v(R_{mn}^p)\, \boldsymbol{\rho}_n^o(\mathbf{r}_n^c)}{R_{mn}^p}\, dS' \pm \right.$$
$$\left. \pm \frac{-2}{s} L_{mn}^{po} \int_{T_n^o} \frac{d_{mn}^v(R_{mn}^p)}{R_{mn}^p}\, dS' \right] = V_m^v , \tag{22a}$$

$$\sum_{n,p,o} \left[\frac{-s}{2} \mathbf{K}_{mn}^{po}(\mathbf{r}_m^c) \cdot \int_{T_n^o} \frac{b_{mn}^v(R_{mn}^p)\, \boldsymbol{\rho}_n^o(\mathbf{r}_n^c)}{R_{mn}^p}\, dS \pm \right.$$
$$\left. \pm \frac{-2}{s} L_{mn}^{po} \int_{T_n^o} \frac{d_{mn}^v(R_{mn}^p)}{R_{mn}^p}\, dS' \right] = V_m^v , \tag{22b}$$

where

$$a_{mn}^v(R_{mn}^p) = \sum_{u=0}^{v} I_{n,u} \cdot \tag{23}$$
$$\cdot \left[\varphi_{u-v}\left(\frac{sR_{mn}^p}{c} \right) + \varphi_{u-v-1}\left(\frac{sR_{mn}^p}{c} \right) \right] ,$$

$$b_{mn}^v(R_{mn}^p) = \sum_{u=0}^{v} \left[I_{n,u} + 2\sum_{k=0}^{u-1} I_{n,k} \right] \cdot \tag{24}$$
$$\cdot \left[\varphi_{v-u}\left(\frac{sR_{mn}^p}{c} \right) - \varphi_{v-u-1}\left(\frac{sR_{mn}^p}{c} \right) \right] ,$$

$$d_{mn}^v(R_{mn}^p) = \sum_{u=0}^{v} \left[I_{n,u} - 2d\sum_{k=0}^{u-1} (-1)^k I_{n,k} \right] \cdot \tag{25}$$
$$\cdot \left[\varphi_{u-v}\left(\frac{sR_{mn}^p}{c} \right) - \varphi_{u-v-1}\left(\frac{sR_{mn}^p}{c} \right) \right] ,$$

$$V_m^v = \int_0^{\infty} V_m(t)\, \varphi_v(st)\, s\, dt . \tag{26}$$

The upper infinite limit in (26) can be replaced by a finite time interval T_t within the incident wave decays to zero.

Now, the equation (22) is gradually solved for different orders v of Laguerre polynomials in the interval $[0, N_L]$, which results in $N \times N_L$ unknown coefficients $I_{n,u}$. In order to solve (22), the inverse matrix has to be computed (once only).

For obtaining an accurate solution, the minimum number of temporal basis functions N_L, and the time scale factor s have to be determined. In order to compute the number of temporal functions N_L, we can follow [4]

$$N_L = 2BT_f + 1 , \tag{27}$$

where B is the bandwidth of the incident wave and T_f is the length of the desired transient response.

The time scale factor should be determined so that a set of weighted Laguerre polynomials can accurately approximate the desired transient response. By our experience for a Gaussian pulse, the time scale factor can be evaluated by

$$s \cong 7B . \tag{28}$$

3.1 Comparing Schemes with Weighted Laguerre Polynomials

Two alternative schemes with weighted Laguerre polynomials have been derived. Now, their properties are going to be compared with the scheme published in [4]:

- For the schemes (22), neither the auxiliary vector [4] as an unknown quantity representing the electric current density, nor the derivative of the electric field intensity of the incident wave is used compared to [4].

- The scheme (22a) is more efficient than [4] or (22b), if additions and subtractions of weighted Laguerre polynomials are computed in advance.

- The efficiency of the schemes (22b) and [4] is identical.

- The accuracy of all the schemes is the same: all the derivations and integrations (with respect to time) both in [4] and in this paper were done analytically.

4. Evaluating Integrals

The accuracy of the method is crucially influenced by the way of evaluating the integrals in (22) or [4]. There are several possibilities of their evaluation:

- Integrals can be computed numerically. The easiest quadratic rules, which are used for a triangular mesh, need to evaluate the integrated functions at least in 9 points [8]. Hence, this approach is very time-consuming in case of using here.
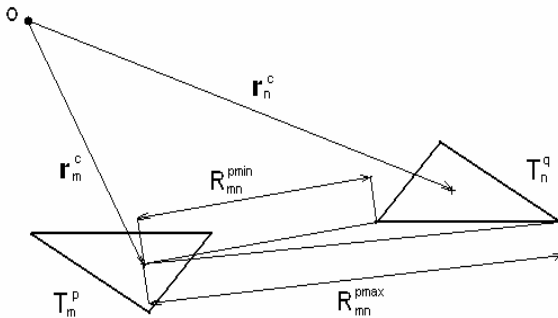
Fig. 3. The definition of the distances $R_{mn}^{p,min}$ and $R_{mn}^{p,max}$.

- The approach used in [4] can be adopted here: the functions (23), (24) and (25) are evaluated in a center of a triangular patch (the assumption of a piecewise constant function over the triangle). Consequently, these constants can be moved out of the integrals. This way of computing is the fastest, but the least accurate one.

The best solution can be composed as a compromise between these two ways: the functions (23), (24) and (25) are constructed using piecewise quadratic polynomials.

4.1 Second-Order Polynomial Approximation

Let be known values of the function $F(x)$ at points $[-\Delta x, 0, -\Delta x]$, then this function can be approximated in the interval $<-\Delta x, -\Delta x>$ by the second-order polynomial [9]

$$F^*(x) = \frac{1}{2\Delta x^2} \left[F(-\Delta x)(x^2 - x\Delta x) - \right.$$
$$\left. - 2F(0)(x^2 - \Delta x^2) + F(\Delta x)(x^2 + x\Delta x) \right]. \quad (29)$$

Using (29), the functions (23), (24) and (25) have to be evaluated in 3 points of a triangular patch: $R_{mn}^{p,min}$, $R_{mn}^{p,cen}$, and $R_{mn}^{p,max}$ (see Fig. 3). The symbol $R_{mn}^{p,min}$ denotes the distance between the centre of the m-th triangle T_m^p and the nearest vertex of the n-th triangle, the symbol $R_{mn}^{p,max}$ denotes the distance between T_m^p and the furthest vertex, and $R_{mn}^{p,cen}$ is the distance of centers of triangles T_m^p and T_n^p.

Now, the functions (23), (24) and (25) can be approximated in the interval $<R_{mn}^{p,min}, R_{mn}^{p,max}>$ by

$$y^{*v}_{mn}(R_{mn}^p) = \frac{1}{2\Delta R_{mn}} \cdot \quad (30)$$

$$\left\{ y^v_{mn}(R_{mn}^{p,min}) \left[(R_{mn}^p - R_{mn}^{p,cen})^2 - (R_{mn}^p - R_{mn}^{p,cen})\Delta R_{mn} \right] \right.$$
$$- 2y^v_{mn}(R_{mn}^{pcen}) \left[(R_{mn}^p - R_{mn}^{p,cen})^2 - \Delta R_{mn}^2 \right] +$$
$$\left. + y^v_{mn}(R_{mn}^{p,max}) \left[(R_{mn}^p - R_{mn}^{p,cen})^2 + (R_{mn}^p - R_{mn}^{p,cen})\Delta R_{mn} \right] \right\},$$

where

$$R_{mn}^{p,cen} = \frac{R_{mn}^{p,max} + R_{mn}^{p,min}}{2} , \quad (31)$$

$$\Delta R_{mn}^p = \frac{R_{mn}^{p,max} - R_{mn}^{p,min}}{2} . \quad (32)$$

The symbol y stands for any function (23), (24) and (25). This approximation has to be applied to compute integrals of functions ρR, ρ, ρ/R, R and $1/R$. Thanks to the approximation, integrals can be computed analytically, [10], [11].
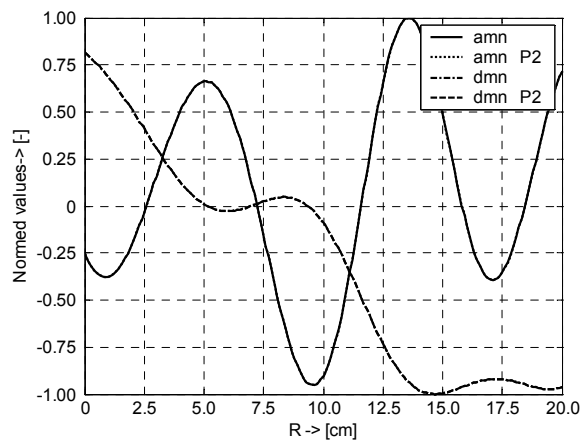
Fig. 4. Approximation of functions a_{mn}^v and d_{mn}^v by the second-order polynomial: $\Delta R_{mn} = 0.5$ cm, P2 denotes the second order polynomial approximation, and $v = 241$.

An example of the approximation of functions $a_{mn}{}^v$ and $d_{mn}{}^v$ by the second-order polynomial is shown in Fig. 4. The functions are a solution of a dipole analysis, which is described below. Functions are depicted for $v = 241$ and normalized. Obviously, the approximation is very accurate.

4.2 First-Order Polynomial Approximation

The first order polynomial approximation is introduced to yield lower CPU-time demands. On the other hand, accuracy of the first-order approximation is not so good.

If values of the function $F(x)$ at the points $[-\Delta x, +\Delta x]$ are known, $F(x)$ can be approximated in $<-\Delta x, +\Delta x>$ by the first-order polynomial

$$F^*(x) = \frac{1}{\Delta x}\left[F(-\Delta x)(\Delta x - x) + F(\Delta x)(\Delta x + x)\right]. \quad (33)$$

In order to use (33), the functions (23), (24) and (25) have to be evaluated in 2 points on a triangular patch: $R_{mn}{}^{p,min}$, and $R_{mn}{}^{p,max}$ (see Fig. 3). The functions (23), (24) and (25) can be approximated in the interval $<R_{mn}{}^{p,min}, R_{mn}{}^{p,max}>$ by the following expression:

$$y^*{}_{mn}^v\left(R_{mn}^p\right) = \frac{1}{\Delta R} \cdot$$
$$\left\{ y^*{}_{mn}^v\left(R_{mn}^{p,min}\right)\left[\Delta R - \left(R_{mn}^p - R_{mn}^{p,cen}\right)\right] + \right. \quad (34)$$
$$\left. + y^*{}_{mn}^v\left(R_{mn}^{p,max}\right)\left[\Delta R + \left(R_{mn}^p - R_{mn}^{p,cen}\right)\right]\right\} .$$

Again, the symbol y stands for any function (23), (24) and (25). The approximation has to be applied to compute integrals of functions ρ/R, R and $1/R$ only. Thanks to the approximation, integrals are computed analytically [10], [11].

An example of the approximation of functions $a_{mn}{}^v$ and $d_{mn}{}^v$ (the same functions as in the previous paragraph) by the first-order polynomial is shown in Fig. 5: the first-order polynomial approximation is less accurate compared to the second-order one. The highest differences appear at the local extremes of functions. Notice that the functions $a_{mn}{}^v$ and $b_{mn}{}^v$ are of the same values but the different forms.
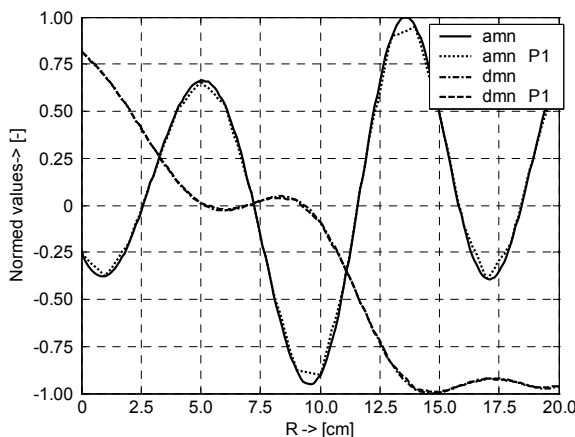
Fig. 5. Approximation of functions $a_{mn}{}^v$ and $d_{mn}{}^v$ by the first-order polynomial: $\Delta R_{mn} = 0.5$ cm, P1 denotes the first-order polynomial approximation, $v = 241$.

4.3 Comparison of Approximations

Now, the accuracy of the approximation of functions $a_{mn}{}^v$ and $d_{mn}{}^v$ by the first- and second-order polynomials is compared to the frequency-domain data in the time- and frequency domain. Frequency domain data, the data obtained by solving the same structure by method of moments in the frequency domain, are considered to be the reference solution, because its credibility is well known [1], [5], [8].

We compare parameters of the strip dipole (Fig. 6) excited by Gaussian voltage source at its center

$$U(t) = U_0 \frac{4}{c_0 T \sqrt{\pi}} e^{-\left[\frac{4}{T}(t-t_0)\right]^2} , \quad (35)$$

where T is the width of the Gaussian pulse, t_0 is a time delay that represents the time distance of the pulse peak from the origin and c_0 is the velocity of the light in free space. The Gaussian pulse is with $U_0 = 120\,\pi$ V, $T^{[LM]} = 0.2$ LM (light-meter), and $t_0^{[LM]} = 0.3$ LM. Note that 1 LM (a light meter) is the unit of time taken by the electromagnetic wave to propagate a distance of 1.0 m in free space. In addition, time variables with or without the superscript [LM] denote units of these variables in light meters or in seconds in this paper.
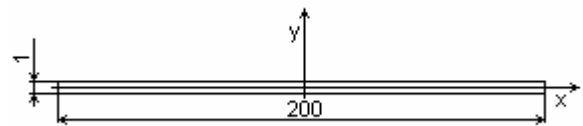
Fig. 6. The analyzed strip dipole.

The dipole is 200 mm long and 1 mm wide. Its surface is modeled by 40 triangles. In the time domain, the response is computed up to $T_t^{[LM]} = 10$ LM, and in the frequency domain, up to $f_{max} = 3$ GHz., $B = 3.6$ GHz . According to the equations (28) and (29), the number of base functions is $N_L = 241$ and the time scale factor is $s = 2.52 \cdot 10^{10}$.

Current responses and input impedance in the center of the dipole are shown in Fig. 7 and Fig. 8, respectively.
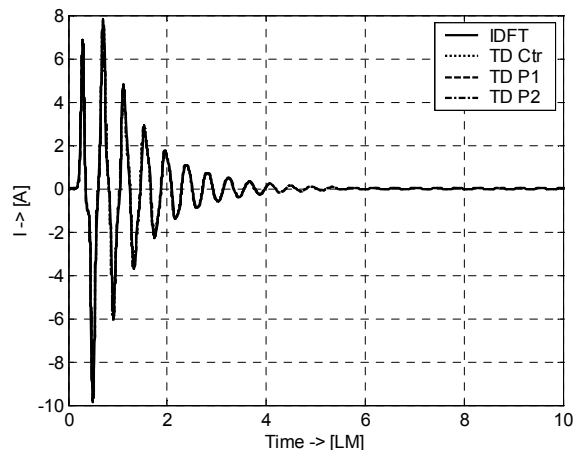
Fig. 7. Transient responses at the center of the dipole.

Abbreviations used in the legend of figures denote:

- FD – the frequency domain data;
- IDFT – the frequency domain data processed by the inverse Fourier transform;
- TD CTr – the time domain solution, the functions (23), (24) and (25) evaluated in triangles centers [4];
- TD P1 – the time domain solution using the first-order polynomial approximation for the functions (23), (24) and (25);
- TD P2 – the time domain solution using the second-order polynomial approximation for the functions (23), (24) and (25).

Fig. 7 confirms that the difference among the transient responses is negligible as assumed.

Applying fast Fourier transform to TD CTr, TD P1, TD P2, and computing the input impedance (Fig. 8), significant differences can be observed at local extremes. The differences can be highlighted when depicting a percentage error (Fig. 9). Obviously, the agreement between the FD solution and the TD P2 one is excellent; the agreement between the FD solution and the TD P1 one is good, whereas the agreement between the FD solution and the TD CTr one is worse. The high percentage errors at low frequencies (0.75 GHz, 1.45 GHz, 2.15 GHz, 2.85 GHz), were expected due to very small reference values (Fig. 9a).
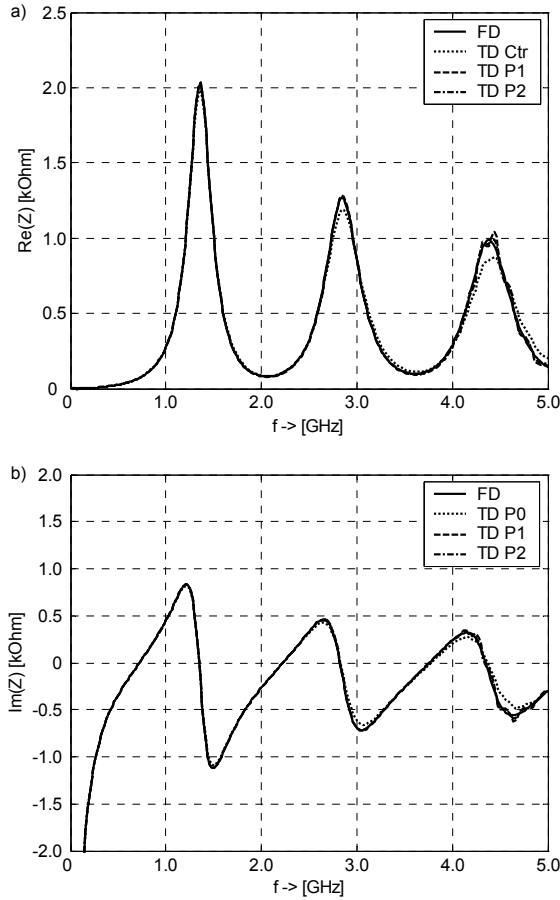
Fig. 8. The input impedance at the dipole center: a) the real part, b) the imaginary part.

5. Modeling Microstrip Structures

In order to model microstrip structures in the time domain, the previous development has to be extended:

- So-far used Green's functions expected the homogeneous surrounding medium with permittivity ε and permeability μ. In case of microstrip structures, free-space Green's functions have to be replaced by layered media ones.

- If an analyzed structure is excited by a microstrip line, a matching termination has to be added.
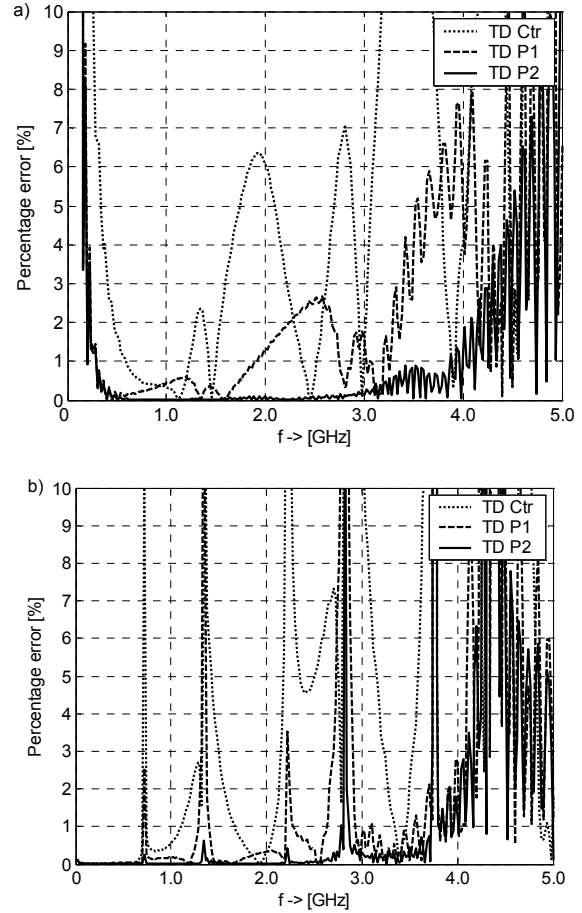
Fig. 9. Percentage error of the input impedance: a) the real part, b) the imaginary part.

5.1 Green's Functions

For modeling one layer substrate, the approximation of Green's function in the frequency domain [12] can be expressed

$$\mathbf{J}(\omega)\, G_A = \mathbf{J}(\omega)\left[\frac{\exp(-jkr_0)}{r_0} - \frac{\exp(-jkr_1)}{r_1}\right], \quad (36)$$

$$\mathbf{J}(\omega)\, G_V = \mathbf{J}(\omega)\cdot$$
$$\cdot\left[\frac{\exp(-jkr_0)}{r_0} - (1-\eta)\sum_{i=1}^{\infty}(-\eta)^{i-1}\frac{\exp(-jkr_i)}{r_i}\right] \quad (37)$$

with

$$\eta = \frac{\varepsilon_r - 1}{\varepsilon_r + 1} \ , \tag{38}$$

$$r_i = \sqrt{(x_m - x')^2 + (y_m - y')^2 + 2ih}, \ \ for \ i = 0, 1, 2 \ ... \infty \ , \tag{39}$$

where G_A and G_V denote Green's function approximations of the vector potential and the scalar one, k is the wave number in the vacuum and h is the height of a substrate. The restrictions of using Green's function approximations (36) and (37) are following:

- The substrate has to be thin: $h / \lambda(f_{max}) < 0.05$;

- The dielectric constant of the substrate has to be lower than 3.

- The substrate is supposed to be infinite in the area.

Using inverse Fourier transform, Green's functions (36) and (37) can be transformed to the time domain

$$IFT\left\{ \mathbf{J}(\omega) G_A \right\} = \frac{\mathbf{J}(t - r_0 / c_0)}{r_0} - \frac{\mathbf{J}(t - r_1 / c_0)}{r_1} \ , \tag{40}$$

$$IFT\left\{ \mathbf{J}(\omega) G_V \right\} = \frac{\mathbf{J}(t - r_0 / c_0)}{r_0} - \\ - (1 - \eta) \sum_{i=1}^{\infty} (-\eta)^{i-1} \frac{\mathbf{J}(t - r_i / c_0)}{r_i} \ , \tag{41}$$

where c_0 is the velocity of the light in the vacuum.

Considering (40) and (41), the equations (22a), (12) and (13) can be rewritten to the form:

$$V_m^v = \sum_{n,p,o} \left\{ \frac{-s}{2} \mathbf{K}_{mn}^{po}(\mathbf{r}_m^c) \cdot \right. \\ \cdot \int_{T_n^o} \left[\frac{a_{mn}^v(R_{0mn}^p)}{R_{0mn}^p} - \frac{a_{mn}^v(R_{1mn}^p)}{R_{1mn}^p} \right] \mathbf{\rho}_n^o(\mathbf{r}_n^c) \, dS' \pm \\ \pm \frac{(-2)}{s} L_{mn}^{po} \left[\int_{T_n^o} \frac{d_{mn}^v(R_{0mn}^p)}{R_{0mn}^p} dS' - \right. \\ \left. \left. - (1 - \eta) \int_{T_n^o} \sum_{i=1}^{\infty} (-\eta)^{i-1} \frac{d_{mn}^v(R_{imn}^p)}{R_{imn}^p} dS' \right] \right\} \ , \tag{22a}$$

$$\mathbf{K}_{mn}^{po}(\mathbf{r}_m^c) = \frac{\mu_0 l_m}{16\pi} \ \mathbf{\rho}_m^p(\mathbf{r}_m^c) \ \frac{l_n}{A_n^o} \ , \tag{12}$$

$$L_{mn}^{po} = \frac{l_m}{4\pi\varepsilon_0} \ \frac{l_n}{A_n^o} \ , \tag{13}$$

where

$$R_{imn}^p = \sqrt{R_{mn}^{p \ 2} + 2ih} \ . \tag{42}$$

A similar procedure can be applied to rearranging (22b).

5.2 Numerical Modeling of Matching Termination

If an analyzed structure is fed by a microstrip line, a matching termination has to be added. The situation is depicted in the Fig. 10, where a device under test is inserted between 2 terminating lines. The device is fed at the reference plane 1. The excitation signal propagates in the form of the forward traveling wave towards the DUT. A part of the signal passes through the DUT, and the rest returns back as a reflected wave. Thanks to the termination, the reflected wave is "absorbed". Without the terminating lines, the next reflected wave would arise at the references plane 1 and also at the reference plane 2.
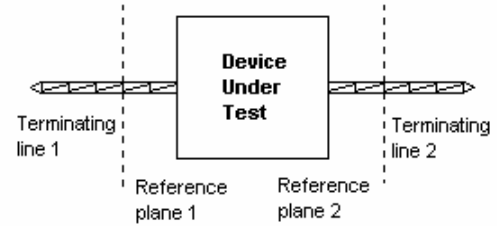
Fig. 10. The device under test inserted between terminating lines.

The idea of numerical imposing matching termination is simple: the current $I(\omega, x)$ propagating along a lossless transmission line 2 can be expressed as a sum of a forward traveling current wave and a backward one [13]

$$I(\omega, x) = I_0^+(\omega) \exp\left(-j \frac{\omega \sqrt{\varepsilon_{eff}}}{c_0} x \right) + \\ + I_0^-(\omega) \exp\left(j \frac{\omega \sqrt{\varepsilon_{eff}}}{c_0} x \right) . \tag{43}$$

On a match-terminated line, there are no reflections from the load, and therefore

$$I(\omega, x) = I_0^+(\omega) \exp\left(-j \frac{\omega \sqrt{\varepsilon_{eff}}}{c_0} x \right) \ , \tag{44}$$

where ε_{eff} is the effective dielectric constant of the microstrip transmission line, which can be evaluated using an empirical formula given in [13].
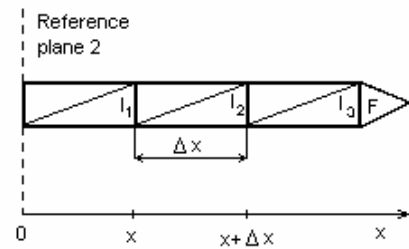
Fig. 11. The terminating line at the port 2.

In order to use the condition (44) in the time domain, the inverse Fourier transform has to be applied

$$I\left(t - \frac{x\sqrt{\varepsilon_{reff}}}{c_0}\right) = I_0^+\left(t - \frac{x\sqrt{\varepsilon_{reff}}}{c_0}\right) \, . \quad (45)$$

If the reference is shifted from zero to a point x on the line, then the current at the point $x+\Delta x$ (Fig. 11) is

$$I\left(t - \frac{(x+\Delta x)\sqrt{\varepsilon_{reff}}}{c_0}\right) = I_x\left(t - \frac{\Delta x\sqrt{\varepsilon_{reff}}}{c_0}\right) \, . \quad (46)$$

The way of matching a termination line to a reference plane is obvious now. E.g., for matching the termination line 2 to the reference plane 2 the following condition can be written:

$$I_k(t) = I_{k-1}\left(t - \frac{\Delta x\sqrt{\varepsilon_{reff}}}{c_0}\right), \text{ for } k = 1, 2, 3. \cdot \quad (47)$$

The relations (47) have to be added to N equations (22). The same procedure can be done for the port 1 (the reference plane 1).

To be notice, the effective dielectric constant of the microstrip ε_{eff} is frequency-dependent. However, the dependence is very weak at low frequencies (up to 5 GHz), and can be neglected.

The triangle face F (Fig. 11) is added to the end of the terminating line in order to make the boundary edge the internal one. However, the face F is not taken into account in the equations (22) for $n = 1, ..., N$.

Once the transient responses are computed at the reference planes and mapped to the frequency domain by Fourier transform, S-parameters of an analyzed structure can be computed in wide range of frequencies.

5.3 Numerical Example

The functionality of the above-described approach is demonstrated by analyzing a microstrip filter (Fig. 12). Time-domain numerical results are mapped to the frequency domain using Fourier transform, and compared to the results of the frequency domain analysis [5], [8].
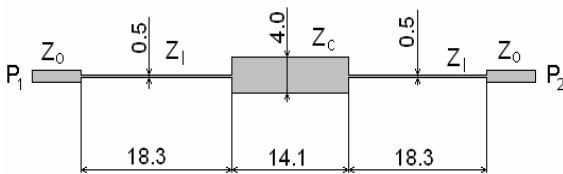
Fig. 12. The analyzed microstrip filter. The height of the substrate is $h = 0.508$ mm and the relative permittivity is $\varepsilon_r = 2.33$. The characteristic impedance of the microstrip line is $Z_0 = 50\ \Omega$.

The analyzed microstrip filter, which is matched at its ends (P_1 and P_2) by matching terminating lines (not depicted in the figure), is excited by a Gaussian voltage source with the following parameters: $U_0 = 120\pi$ **V**, $T^{[LM]} = 0.2$ LM, and $t_0^{[LM]} = 0.3$ LM. In the time domain, the responses are computed up to $T_t^{[LM]} = 1.5$ LM, and in the frequency domain, up to $f_{max} = 3$ GHz, $B = 3.6$ GHz. According to the equations (28) and (29), the number of basis functions is $N_L = 37$, and the time scale factor is $s = 2.52 \cdot 10^{10}$.

The calculated transient responses at the ends (IP_1 and IP_2) of the filter are depicted in Fig. 13. For obtaining S-parameters, a forward traveling current wave at the microstrip line of the characteristic impedance Z_0 has to be determined. There are two approaches:

- Analytical: The waveform of the forward traveling wave is known (Gaussian pulse here), and therefore, only the amplitude has to be determined by considering of the value of the characteristic impedance Z_0.

- Numerical: A microstrip line guiding a forward traveling wave is analyzed by the same method like the microstrip filter. If a microstrip line is matched at both ends, only a forward traveling wave exists.

The first approach is faster and usually less accurate than the second one. The differences lie in the delay and amplitude of Gaussian pulse. It is better to simultaneously solve two problems by the same method, than applying two different methods. E.g., if the forward current wave propagating along the microstrip line is determined numerically, the peak of Gaussian pulse lies at $t^{[LM]} = 0.298$ LM instead of $t^{[LM]} = 0.3$ LM. A similar shift can be expected in case of the transient responses of the analyzed filter
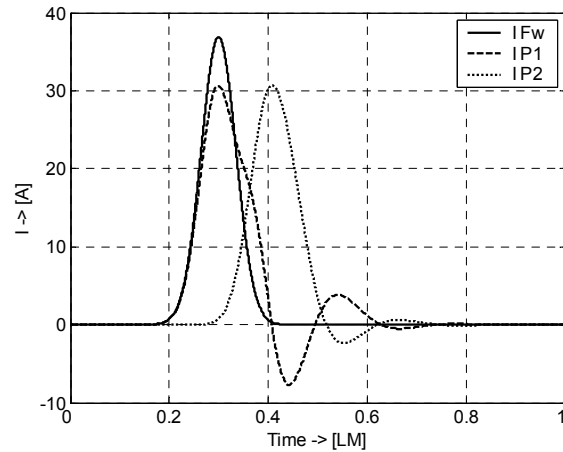
Fig. 13. Transient responses of the analyzed microstrip filter (IP_1 and IP_2) and of forward traveling current wave at microstrip line of characteristic impedance $Z_0 = 50\ \Omega$ (IFw).

Once the forward traveling current wave is determined (Fig. 13, IFw), numerically in this example, S-parameters can be computed using the following expressions:

$$S_{11} = -\frac{FFT\{IFw\}}{FFT\{IP_1 - IFw\}} \, , \quad (48)$$

$$S_{21} = -\frac{FFT\{IP_2\}}{FFT\{IFw\}} \, . \quad (49)$$

The calculated S-parameters are depicted in Fig. 14. Obviously, our solutions meet very well the results calculated directly in the frequency domain.

6. Conclusions

In this paper, alternative schemes with weighted Laguerre polynomials have been developed. For these schemes, neither the Hertz vector as the unknown variable instead of the electric current density, nor the derivative of the incident electric wave are used in the comparison to [4]. The accuracy of both schemes is the same as the scheme published in [4]. In addition, one of these schemes is more efficient than [4], if the addition and subtraction of weighted Laguerre polynomials are computed in advance.
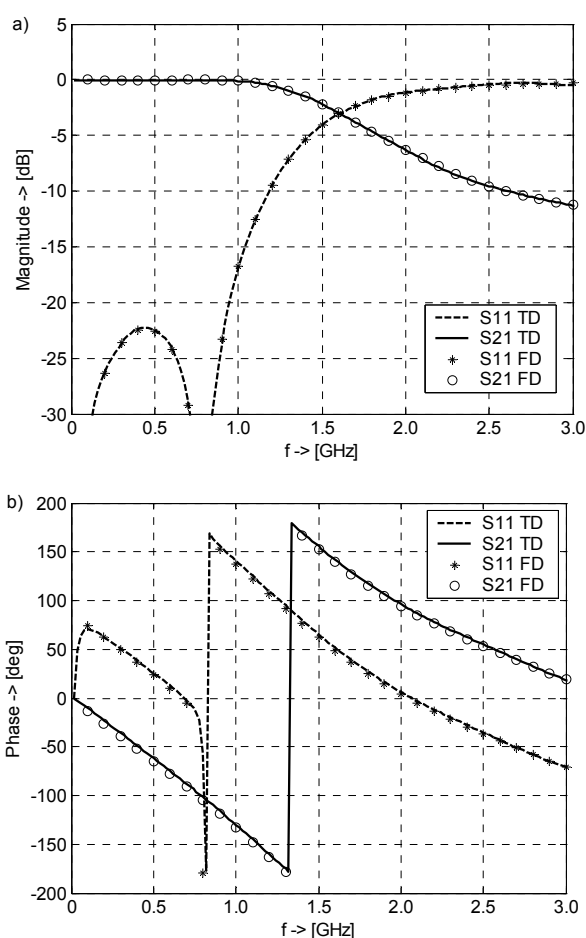
Fig. 14. S-parameters of analyzed microstrip filter: a) magnitude, b) phase.

An efficient and accurate way of evaluating integrals of Green's functions was proposed using the first- and second-order polynomial approximation of sums of weighted Laguerre polynomials. For reaching accuracy up to 3%, the first-order polynomial approximation is satisfactory.

In the last part of the paper, the time domain modeling of microstrip structures was discussed. The matching conditions for microstrip lines in the time domain were introduced. The proposed approach was verified on the analysis of the microstrip filter, and the results were compared to the frequency domain solutions. The comparisons show functionality of the proposed approach, and a very good fit.

Acknowledgements

References

[1] RAO, S. M. *Time Domain Electromagnetics*. London: Academic Press, 1999.

[2] RAO, S. M., SARKAR, T. K. Numerical solution of time domain integral equations for arbitrarily shaped conductor/dielectric composites bodies. *IEEE Transactions on Antennas and Propagation.* 2002, vol. 50, no. 12, p. 1831–1837.

[3] LACIK, J., RAIDA, Z., MOTL, M. TD-EFIE with 3-point backward difference and stability investigation. *WSEAS Transactions on Computers.* 2004, vol. 3, no. 6, p. 1877–1881.

[4] CHUNG., S., SARKAR, T. K., JUNG, B. H., SALZAR-PALMA, M., JI, Z., JANG, S., KIM, K. Solution of time domain electric field integral equation using the Laguerre polynomials. *IEEE Transactions on Antennas and Propagation.* 2004, vol. 52, no. 9, p. 2319–2328.

[5] RAO, S. M., WILTON, D. R., GLISSON, A. W. Electromagnetic scattering by surfaces of arbitrary shape. *IEEE Transactions on Antennas and Propagation.* 1982, vol. 30, no. 5, p. 409–418.

[6] POULARKIS, A. D. *The Transforms and Applications Handbook*. Piscataway: IEEE Press, 1996.

[7] LACIK, J., RAIDA, Z. Transient analysis of scatterers and antennas: Laguerre polynomials scheme with improved efficiency. In *Proc. of the International Conference on Electromagnetics in Advanced Applications ICEAA 2005*. Turin (Italy): Polytecnico di Torino, 2005, p. 257–260.

[8] MAKAROV, S. MoM antenna simulations with Matlab: RWG basis functions. *IEEE Antennas and Propagation Magazine.* 2001, vol. 43, no. 5, p. 100–107.

[9] LACIK, J. Modelling of antennas in the time domain using Laguerre polynomials. In *Proceedings of STUDENT EEICT 2005*. Brno: Brno University of Technology, 2005, p. 426–430.

[10] WILTON, D. R., RAO, S. M., ALLEN, W. Potential integrals of uniform and linear source distributions on polygonal and polyhedral domains. *IEEE Transactions on Antennas and Propagation.* 1984, vol. 32, no. 3, p. 276–281.

[11] EIBERT, T. F., HANSEN, V. On the calculation of potential integrals for linear source distributions on triangular domains. *IEEE Transactions on Antennas and Propagation.* 1995, vol. 43, no. 12, p. 1499–1502.

[12] MOSIG, J., R. Analytical and numerical techniques in the Green's function treatment of microstrip antennas and scatterers. *Proceedings of IEE.* 1983, vol. 130, no.2, p. 175–182.

[13] POZAR, D. M. *Microwave Engineering*. New York: J. Wiley and Sons, 2005.